Summary: Hybrid organic-inorganic nanocomposites containing hyperbranched structures were prepared through a dual-curing process, which involves photopolymerization and condensation alkoxysilane groups. In particular, an oligomer containing PEO units and α,ω-methacrylate groups was used together with a HBP bearing acrylic groups as the organic phase precursors. MEMO, as the organic-inorganic linker, and TEOS, as inorganic phase precursor, were also employed. The kinetics of both photopolymerization and condensation reactions were investigated by double bond conversion analysis (via FT-IR) and weight loss determination, respectively. The mobility of the organic phase was studied by means of DSC and DMTA and correlated with hybrid composition. TEM analyses performed on microtomed film slices indicated the formation of nanoscale silica domains. Hybrids were coated onto an LDPE film previously subjected to a plasma treatment, and substrate-coating interfacial adhesion was investigated through stress-strain and DMTA experiments.

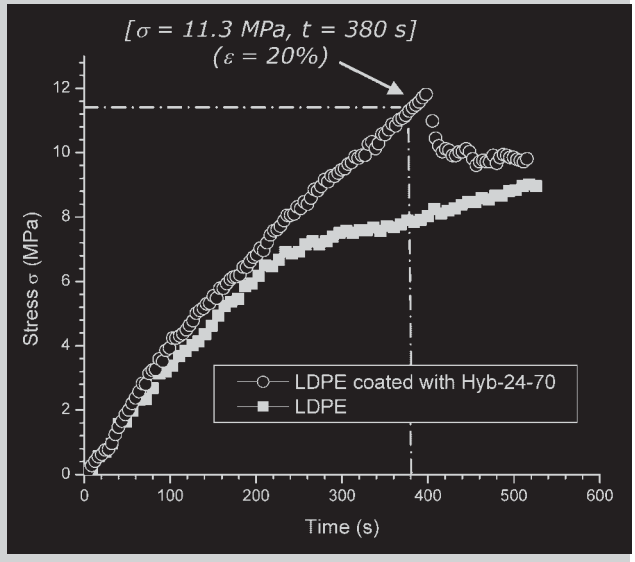

Stress versus time plot of LDPE and LDPE coated with Hyb-24-70 at 4.5×10^{-3} s^{-1}.

Preparation and Characterization of Hybrid Nanocomposites Coated on LDPE

Laura Mazzocchetti,[1] *Mariastella Scandola,**[1] *Ezio Amerio,*[2] *Giulio Malucelli,*[2] *Claudia Marano*[3]

[1]Università di Bologna, Dipartimento di Chimica ''G. Ciamician'' and INSTM UdR Bologna, Via Selmi 2, 40126 Bologna, Italy
Fax: +39 051 209 9456; E-mail: mariastella.scandola@unibo.it
[2]Politecnico di Torino, Dipartimento di Scienza dei Materiali ed Ingegneria Chimica and INSTM UdR Torino, C.so Duca degli Abruzzi 24, 10129 Torino, Italy
[3]Politecnico di Milano, Dipartimento di Chimica, Materiali e Ingegneria Chimica and INSTM UdR Milano, Piazza Leonardo da Vinci 32, 20133 Milano, Italy

Received: July 28, 2006; Revised: September 6, 2006; Accepted: September 7, 2006; DOI: 10.1002/macp.200600389

Keywords: adhesion; coatings; hyperbranched polymers; organic-inorganic hybrids

Introduction

In the last decade new materials with a nanophase structure, composed of strictly interconnected organic and inorganic phases (the so-called hybrids or ceramers), were developed.[1–3] These materials combine the attractive properties of ceramics such as high modulus, thermal stability and low coefficient of thermal expansion, with the high ductility and low temperature processing conditions typical of polymers.

The nanophase morphology strongly affects properties and behavior of the hybrids. These materials are very interesting for applications in diversified fields such as optics, mechanics, electronics, biomedicine, etc.[4] At present, their main commercial applications are in the area of protective coatings of both organic and inorganic substrates. Recently, ceramers are also proposed for packaging applications.[5]

Hybrids based on silica are the most widely investigated, though alternative metal oxides, such as those of titanium,

zirconium, aluminum and cerium, can be used.[6] A number of different organic polymers have been investigated as constituents of the ceramer organic phase.[6–9] The preferred procedure for the synthesis is the sol-gel process. It is based on two steps involving hydrolysis and condensation reactions starting from metal alkoxides. By this synthetic pathway, it is possible to prepare interconnected organic-inorganic networks that may result in dispersed nanostructured phases.

A recently developed alternative for ceramer production is the combination of UV curing with the sol-gel reaction. By this procedure, nanostructured coatings with improved mechanical, electrical and optical properties as well as scratch, abrasion, heat and radiation resistance were obtained.[10–12]

In this context, we earlier reported the synthesis and characterization of new hybrid systems obtained through the mentioned dual-curing process, using an organic poly(ethylene oxide) (PEO)-based dimethacrylate oligomer precursor (BEMA 1400), tetraethoxysilane (TEOS) and methacryloyloxypropyltrimethoxysilane (MEMO) as the interphase agent.[13,14] The hybrids were nanostructured, transparent and thermally stable.[13] When coated on poly(ethylene terephthalate) (PET), they showed good adhesion to the substrate.[14]

The aim of this work is to extend the study of ceramer synthesis via double curing, by incorporating in the reaction mixture a hyperbranched polymer (HBP) bearing acrylic groups. It is well known that the use of HBPs with densely branched structures and a large number of reactive end-groups is very attractive, especially for coating and thermoset applications. HBP structures in thermoset formulations allow to enhance system reactivity and to improve properties such as viscosity, solubility and adhesion.[15,16] Hyperbranched polyesters with acrylate, vinyl ether, allyl ether, or epoxy functionalities have been employed as multifunctional crosslinkers in coatings and in thermosets obtained by either thermal or UV-curing methods. In the field of photopolymerization, their introduction concerns both radical and cationic processes.[17–22] For these reasons, our attention was focused on the influence of HBP structures on the kinetics of the UV-curing process and on the adhesion of double-cured organic-inorganic hybrids onto low-density polyethylene (LDPE). Mobility of the organic phase during the various steps of hybrid synthesis and adhesion of the ceramer to the LDPE substrate were investigated by DSC, DMTA and mechanical measurements.

Experimental Part

Materials

Bisphenol A ethoxylate (15 EO/phenol) dimethacrylate (BEMA 1400), MEMO, TEOS, hydrochloric acid and dibutyltin diacetate (condensation catalyst) were purchased from Aldrich. The structure of BEMA 1400 is reported in Figure 1, together with the structure of the HBP, that was kindly supplied by Perstorp Specialty Chemicals (Sweden); $\overline{M}_n = 1\,560$; $\overline{M}_w = 2\,980$; acrylic functionality $= 5.6$ mmol $\cdot$ g^{-1}; viscosity (23 °C) $= 120$ Pa $\cdot$ s. The photoinitiator was 2-hydroxy-2-methyl-1-phenylpropan-1-one (Darocur 1173 from Ciba Specialty Chemicals). Films of LDPE (Polimeri Europa, Milano; thickness: 45 μm) were used as a supporting surface for the hybrid coatings. Prior to coating, the LDPE film was submitted to plasma treatment (gas: air) using a 13.56 MHz radio-frequency reactor, Plasmod 1645, supplied by March Instruments Inc. The reactor pressure was 0.1 Torr (≈13 Pa), the gas flow rate was 7.7 cm^3 $\cdot$ min^{-1}, the power was set at 15 W and the treatment time was 2 min.

Preparation of the Hybrids

A typical UV-curable mixture was prepared by mixing 56% BEMA 1400 oligomer with 24% HBP and 20% MEMO, then

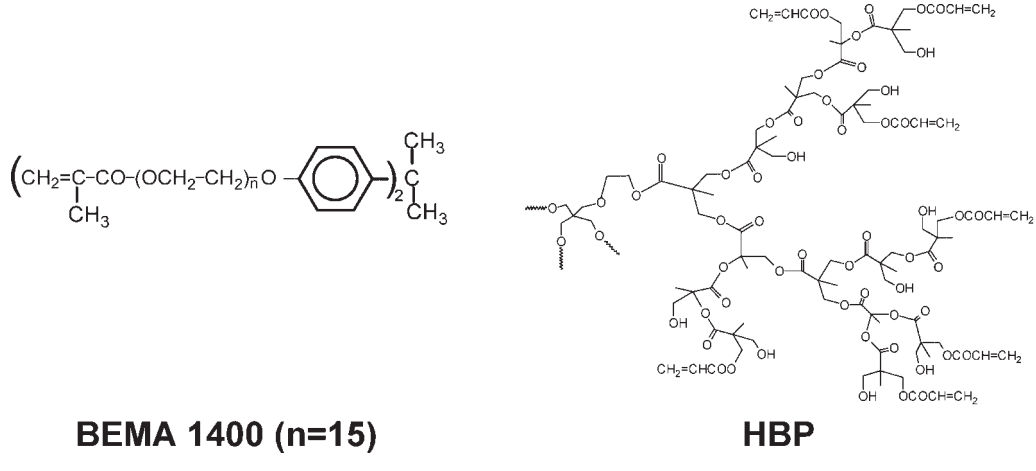

Figure 1. Structure of BEMA 1400 oligomer and of the HBP.

adding TEOS (in different amounts, up to 70% of the final mixture weight), 4% Darocur 1173 as photoinitiator, water (with a constant alkoxy/water molar ratio equal to 2) and 2% of both dibutyltin diacetate and concentrated HCl, as condensation catalysts (all compositions are expressed as weight fractions). The final mixture was then coated on the plasma-treated LDPE substrate by means of a wire wound applicator in order to control coating thickness. Labels used to indicate the different reactant mixtures and products are reported in Table 1.

The photochemical curing was performed at room temperature by using a medium vapor pressure Hg UV lamp (Helios Italquartz, Italy), with radiation intensity on the surface of the sample of 20 $mW \cdot cm^{-2}$, working in N_2 atmosphere; the reaction time was changed up to a maximum of 120 s. The subsequent condensation reaction was performed by keeping the photocured films in an oven at 75 °C for 4 h. Earlier results[13] showed that this time was sufficient to guarantee completion of the condensation process.

The same dual curing procedure was adopted to prepare 'free-standing' ceramer films. An inert substrate was used as the support for the reaction mixture, from which films were easily recovered after the curing and condensation reactions.

All prepared hybrids were transparent and X-ray diffraction analyses evidenced their totally amorphous structure.

Characterization Techniques

The kinetics of the photopolymerization process was investigated by real-time FT-IR spectroscopy, using a Thermo-Nicolet 5700 apparatus. The liquid formulations were coated onto a silicon wafer. The sample was exposed simultaneously to the UV beam which induces polymerization, and to the IR beam which analyzes the extent of the reaction in situ. Since IR absorbance is proportional to monomer concentration, conversion versus irradiation time profiles can be obtained. Methacrylic group conversion was followed by monitoring the decrease of methacrylic groups absorbance at 1 630 cm^{-1}. This band intensity was normalized to that of the C=O signal located at 1 700 cm^{-1}. The condensation reaction was monitored by measuring the weight loss due to alcohol evaporation as a function of reaction time. After the dual-curing process, the gel content values (determined by measuring the weight loss of the samples contained in a metal net after 24 h of extraction at room temperature with $CHCl_3$), were found to be always higher than 95%.

DSC measurements were performed using a TA DSC-Q100 apparatus, equipped with a liquid nitrogen cooling system (LNCS) accessory. The samples (about 5 mg) were placed in an open Al pan in order to allow the loss of volatile products during the first heating scan. All samples were subjected to heating runs at 20 °C · min^{-1} in He atmosphere from −120 to 70 °C. Quench cooling was applied between heating scans. T_g values were taken at half-height of the stepwise heat capacity increase at the glass transition.

Mechanical tests were carried out on LDPE films (both uncoated and hybrid coated) in order to evaluate the deformational behavior of the coated material. The thicknesses of the PE film and of the coating layer were about 45 and 15 μm, respectively. Uniaxial tensile tests were performed at room temperature under constant strain rate , at a crosshead speed of 0.3 $mm \cdot min^{-1}$, using an electromechanical dynamometer (MiniMat-Polymer Laboratories). Specimens were cut to proper geometry (Figure 2) in order to localize the material deformation in the central zone of the specimen. An ink spot was placed on the sample's surface in the central zone to measure strain. Strain was obtained as the ratio, d/d_0 between the actual and initial spot diameters ($d_0 \approx 500$ μm). From these strain measurements, it was found that a strain rate of 4.5×10^{-3} s^{-1} was applied to the central zone of the specimen.

Diameter values were determined by using a Nikon phototube (ranging from 150 to 700× in magnification) applied onto a Nikon D70 reflex digital camera for image acquisition. A light-transmission configuration was adopted. It was not always possible to carry out the strain measurement up to the end of the test.

Dynamic mechanical measurements were carried out from −150 to 100 °C by means of a DMTA MkII (Polymer Laboratories Ltd.), using the dual cantilever geometry at a frequency of 3 Hz and 3 °C · min^{-1} heating rate. In order to perform the measurement in bending mode, both on the 'free' hybrid films and on LDPE coated with hybrids, rectangular aluminium plates (dimensions: $5 \times 40 \times 0.6$ mm^3) were used to sandwich the film samples.[14] The sandwich contained one hybrid film between two aluminium plates in the case of the free-standing samples, while for the ceramers coated on LDPE the sandwich was prepared by alternating two films with three aluminium plates, in order to enhance the signals of the hybrid coating.

RX measurements were performed using a Siemens D5000 diffractometer with the Cu K_α radiation ($\lambda = 0.15406$ nm). TEM analyses were performed using a Philips 2010 microscope on microtomized specimens without any specific

Table 1. Labeling system.

Label[a]	Composition[b]
BEMA 1400	Plain methacrylate oligomer
BEMAM	Mixture of BEMA 1400 (80%) with MEMO (20%)
BEMAM-HBP-*x*	Mixtures of BEMAM with HBP (*x* is the HBP percentage in the mixture)
Hyb-*x*-*y*	Final hybrid, where *x* is defined above and *y* is the TEOS percentage in the reaction mixture

[a] The label only accounts for mixture composition. The pertinent curing reactions are specified in the text.
[b] Weight composition.

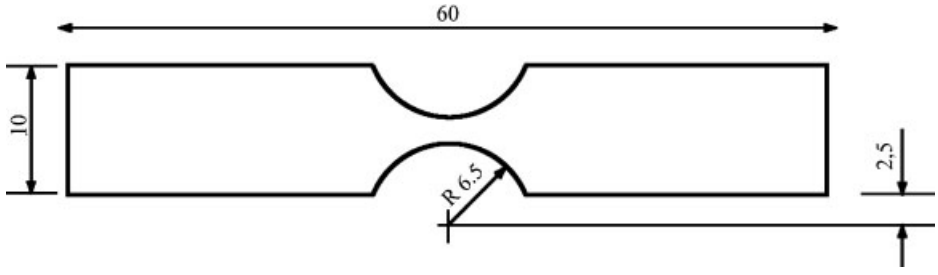

Figure 2. Geometry and dimensions (in mm) of the samples used in tensile test.

staining. Pencil hardness was evaluated on the cured coatings according to the standard test method ASTM D 3363.

Results and Discussion

Kinetics of the Photopolymerization Process

In Figure 3, the kinetic curves of the photopolymerization process of BEMAM-HBP-*x* mixtures containing different amounts (*x*, %) of hyperbranched oligomer are reported. All curves show an asymptotic trend, reached after different irradiation times. An increase in the slope of the kinetic curves was observed in the presence of the HBP oligomer that clearly accelerates the photopolymerization reaction. This behavior is attributed to the large amount of acrylic double bonds in the hyperbranched compound. The curves in Figure 3 also show that, when HBP concentration in the UV-curable mixture is between 0 and 50% w/w, the final double bond conversion is practically complete (around 100%). Conversely, when the amount of HBP is 80 wt.-% or higher, the final double bond conversion is lower. This observation is ascribed to the high crosslink density that rapidly develops in these conditions, which affects polymer segmental mobility and promotes early vitrification phenomena, leading to incomplete conversion (ca. 80%).[15]

Figure 4 shows the kinetics of the photocuring reaction of BEMAM (without HBP) in the presence of different amounts of TEOS (10–70 wt.-%). The photocuring kinetics of plain BEMAM is also shown for the sake of comparison. The presence of TEOS in the UV-curable mixtures causes a decrease in the initial slope of the curves in Figure 4, indicating the slowing down of the double bond conversion process, likely to be due to the dilution of the reactive groups. It is interesting to note, however, that at intermediate irradiation times (20–30 s), an increase in photopolymerization rate is observed with increasing TEOS content. This observation may be attributed to partial condensation reaction of TEOS with MEMO, giving rise to dimers or higher MEMO oligomers. These products,

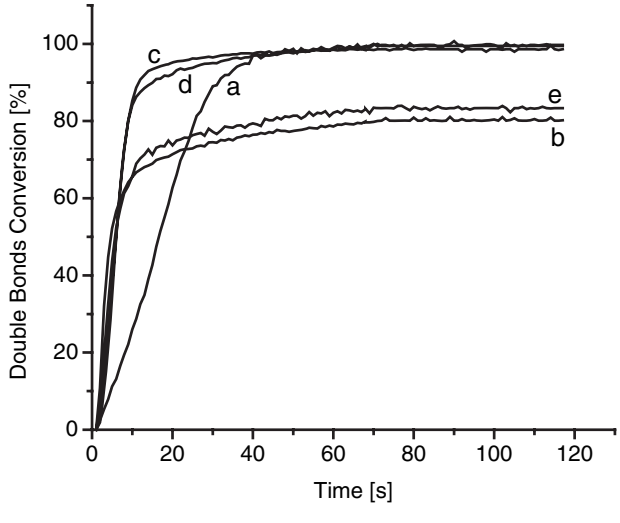

Figure 3. Kinetic curves of the photocuring process (double bond conversion) of BEMAM (a), of plain HBP (b) and of BEMAM-HBP-*x* mixtures with different HBP (*x*, %) content: BEMAM-HBP-20 (c), BEMAM-HBP-50 (d), BEMAM-HBP-80 (e).

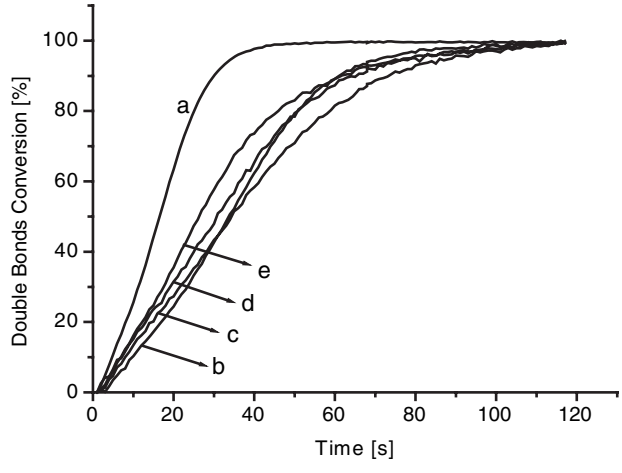

Figure 4. Kinetic curves of the photocuring process of BEMAM containing different amounts of TEOS: (a) 0, (b) 10, (c) 30, (d) 50, (e) 70 wt.-%.

having a high acrylic functionality, could have a similar accelerating effect on the curing rate as that shown above for HBP (Figure 3).

Kinetics of the Condensation Process

The condensation reaction was followed by measuring the weight loss associated with the evaporation of the reaction byproducts. In Figure 5 some representative condensation curves of BEMAM-HBP-20 with different amounts of TEOS are reported. In all the systems investigated, the asymptotic plateau value of the condensation curves is achieved after 4 h treatment in an oven at 75 °C. The measured weight loss is slightly lower than that expected for complete (stoichiometric) conversion of all available alkoxy moieties (19, 27, and 41 wt.-% for Hyb-20-10, Hyb-20-30 and Hyb-20-50 samples, respectively). The observed difference is attributed to the occurrence, during the UV-curing step, of premature condensation reactions involving TEOS and MEMO as suggested above. As a consequence, the total number of curing events that can occur during the condensation step, and the associated weight loss, decreases.

Surface Hardness

Surface hardness of the final double-cured hybrids was determined by the pencil test. For Hyb-24-30, Table 2 compares pencil hardness of the final double-cured ceramer with that of the photocured products of the preliminary steps of hybrid formation. Hardness is not seen to change appreciably up to the final condensation step, where the hard silica particles form and chemically bind the organic phase.

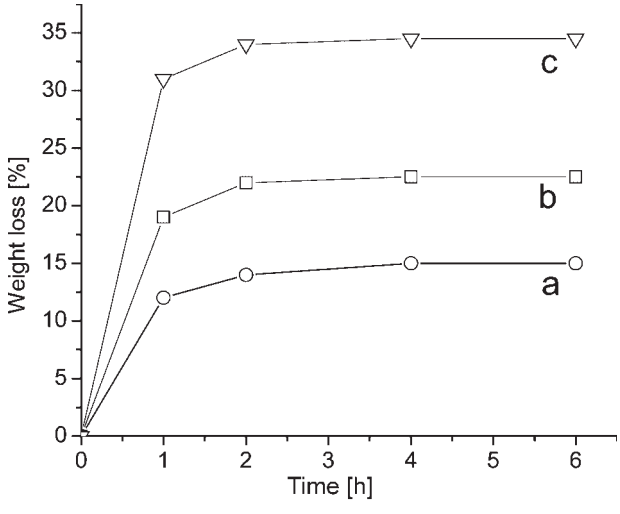

Figure 5. Kinetic curves of the condensation reaction at 75 °C for mixtures of BEMAM-HBP-20 with different amounts of TEOS: 10% (a, Hyb-20-10); 30% (b, Hyb-20-30); 50% (c, Hyb-20-50).

Phase Morphology

In Figure 6(A), a typical TEM micrograph of Hyb-24-30 shows that phase separation in this system occurs at nanoscale level. Silica-rich domains, with average dimension about 40 nm, are observed. Their size is unaffected by the amount of TEOS used in the hybrid formulation. Comparison with earlier results on analogous hybrids without HBP[13] reveals that the addition of HBP does not change the average silica particle size. The Si mapping by EDS [Figure 6(B)] shows that the highest Si content is located in the darker spots of the TEM image, though some Si was also revealed all over the surface.

Mobility of the Organic Phase and Adhesion of the Hybrid to LDPE

The thermal and viscoelastic behavior of the hybrids and of their precursors was investigated by DSC and DMTA. Both techniques were recently shown to be particularly suited to the investigation of changes of organic phase mobility in ceramers.[13,14]

Here, we report results on the hybrid Hyb-24-30, obtained by photocuring and thermally treating 4 h at 75 °C a mixture of 70% BEMAM-HBP-24 with 30% TEOS. Additional samples, obtained by UV-curing individual hybrid components and some of their mixtures were also analyzed for the sake of comparison. Hence, in addition to Hyb-24-30, the following photocured compounds were investigated as constituents of the organic part of the final ceramer: (a) plain BEMA 1400, (b) a mixture of BEMA 1400 and HBP (70/30 w/w, no MEMO) and (c) BEMAM-HBP-24.

Figure 7 compares the DSC curve (d) of the final hybrid Hyb-24-30 with those of the above mentioned samples (a), (b) and (c). Each DSC curve shows a stepwise increase, accounting for the presence of a glass transition, whose temperature (T_g), intensity (ΔC_p) and width (ΔT_g) are reported in Table 2. A clear trend is observed: T_g gradually shifts from −42 °C in BEMA 1400 to −17 °C in Hyb-24-30; in parallel the transition intensity drops from 0.77 to 0.37 $J \cdot g^{-1} \cdot K^{-1}$, and the transition width broadens from 8 to 29 °C.

Comparison of curves (a) and (b) in Figure 7 shows that addition of HBP to BEMA 1400 before photopolymerization results in an overall chain mobility limitation revealed by the increase in both T_g and ΔT_g. This behavior is ascribed to the multifunctionality of HBP reactant which favors crosslinking. T_g increases because mobilization of the crosslinked constrained chain segments requires higher temperatures, and the transition broadens due to increased chain length heterogeneity between crosslinks, which widens the relaxation time distribution.

MEMO addition to the previous mixture causes a further increase of T_g and ΔT_g (curve c and Table 2). This

Table 2. Thermal properties (by DSC and DMTA) and hardness (by pencil test).

Sample	DSC[a]			DMTA	Hardness
	T_g	ΔT_g[b]	ΔC_p	T_α	
	°C	°C	$J \cdot g^{-1} \cdot K^{-1}$	°C	
BEMA1400[c]	−42	8	0.77	−36	4B
70% BEMA1400 + 30%HBP[c]	−38	15	0.58	−30	4B
BEMAM-HBP-24[c]	−31	21	0.44	−20	4B
Hyb-24-30[d]	−17	29	0.37	−14	B

[a] First heating scan.
[b] Temperature interval between the intercepts of the baseline before and after the transition with the tangent to the step.
[c] UV-cured.
[d] Dual-cured (UV and condensation).

observation may appear surprising because, unlike the previously introduced HBP, MEMO is not a multifunctional cross-linking agent, but only bears one methacrylic functionality that can be involved in the photopolymerization process. No additional UV-induced crosslinks are expected in this case. The observed T_g increase is therefore tentatively attributed to partial sol-gel reactions occurring during photocuring at room temperature, a hypothesis already put forward in connection with the deficient weight loss observed in the condensation experiments of Figure 5. In the present case, however, given the absence of TEOS, only the MEMO component should be involved in the reaction. This hypothesis is strengthened by the broad endotherm, appearing in curve (c) of Figure 7 above room temperature. This endothermal behavior (absent in subsequent DSC heating runs) may be associated with methanol release from the methoxysilane moieties of MEMO that undergo further sol-gel reactions during the first DSC scan. Analogous behavior is not expected and indeed is not observed in Figure 7 in either BEMA 1400 or BEMA 1400/HBP mixture, where the components are unable to undergo sol-gel reactions.

Addition of TEOS to the aforementioned mixtures and completion of the dual curing procedure by the high temperature treatment leads to the final Hyb-24-30 ceramer (curve d in Figure 7). In the hybrid, the UV-cross-linked organic phase binds via the MEMO linker, to silica particles. The anchoring effect of the inorganic Si–O–Si network further restricts polymer chain mobility and the glass transition temperature increases (compare curves c and d).

The same samples investigated by DSC were analyzed by DMTA using small aluminium plates to provide a convenient support for the measurement of films in bending mode,[14] and the loss factor curves are reported in Figure 8. The DMTA spectra of all analyzed samples show a main relaxation process (α) and a lower-temperature secondary dissipation region (β). The α relaxation gradually moves to a higher temperature and undergoes intensity and width changes when the composition of the photocured samples changes and the sol-gel reaction leads to the final Hyb-24-30.

The α-peak temperature (T_α, Table 2) displays the same increasing trend as that shown by the calorimetric T_gs. The curves in Figure 8 also show that when sample composition changes from plain BEMA 1400 to the final hybrid Hyb-24-30, the α relaxation widens and the intensity decreases, as a consequence of the enhanced cross-link density that limits molecular mobility and broadens the relaxation time spectrum.

The DMTA spectra in Figure 8 also display a secondary mechanical loss region, whose temperature location roughly corresponds to that given in the literature for the local motion relaxation of PEG,[23] and appears to be unaffected by sample composition. The latter parameter, however, seems to influence the peak intensity in a peculiar way: the peak remains unchanged upon moving from BEMA 1400 to BEMA 1400/HBP photocured mixtures, whereas it increases when MEMO is added to the previous composition before UV-curing, and increases even more in the final hybrid. This observation cannot be related to an increased amount of PEG units undergoing the transition, since none of the above mentioned composition changes (MEMO and TEOS addition) leads to an increase of the PEG fraction. This intensification of the low temperature relaxation process may thus be tentatively ascribed to local mobility of molecular groups introduced by MEMO and TEOS and their oligomeric intermediates and/or to local motion of some absorbed water, which is known to give rise to low-temperature relaxations in the temperature range of interest.[24–26]

The dynamic-mechanical technique was also applied in this work to investigate adhesion between a film substrate and a hybrid used as coating, according to a recently proposed methodology[14] that takes advantage of the use of metal plates to sandwich the film samples and compares

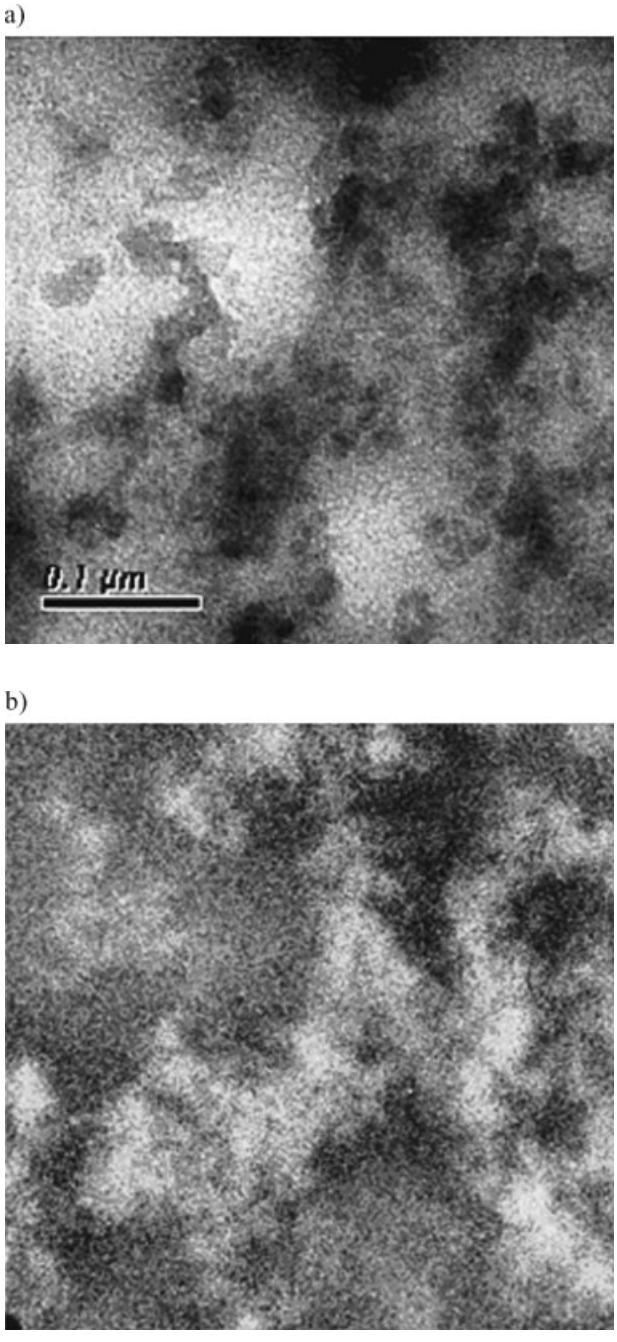

Figure 6. TEM micrograph (a) and EDS Si-mapping (b, Si = lighter spots) of Hyb-24-30.

the viscoelastic spectrum of the free ceramer with that of the ceramer-coated support. The spectral differences observed are then interpreted in terms of molecular interactions at the hybrid-substrate interface.

The LDPE film used in this work as coating substrate was preliminarily subjected to a plasma treatment (see *Experimental Part*) in order to increase polarity and favor coating adhesion. Wettability measurements run with bidistilled water, showed that the contact angle value of LDPE

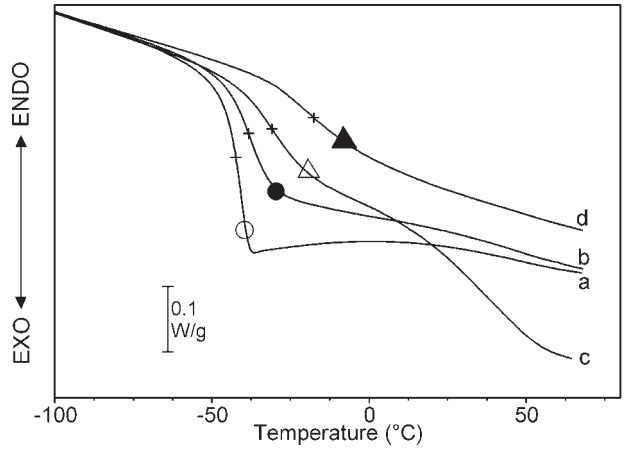

Figure 7. DSC curves of photocured BEMA1400 (○, a); of the photocured mixture BEMA1400/HBP (70/30 w/w) (●, b); of photocured BEMAM-HBP-24 (△, c) and of the final hybrid Hyb-24-30 (▲, d), after the dual photocuring and sol-gel reaction. The glass transition temperature is marked by a cross on the curves.

changed from 95 to 30° immediately after plasma treatment. Upon storage at room temperature, the contact angle slightly increased reaching a constant 40° value after 24 h. This LDPE film was used in coating experiments.

Figure 9 compares the relaxation spectrum of the free hybrid Hyb-24-30 (same curve as that reported in Figure 8) with the spectrum of the hybrid coated on LDPE. The DMTA curve of the plain LDPE supporting film is also shown in Figure 9 for the sake of comparison. Quite disappointingly, the loss region of plasma-treated LDPE is seen to fall in the same temperature range as the main (α) relaxation of the hybrid. Overlapping of dissipation phenomena call for some caution in the results interpretation.

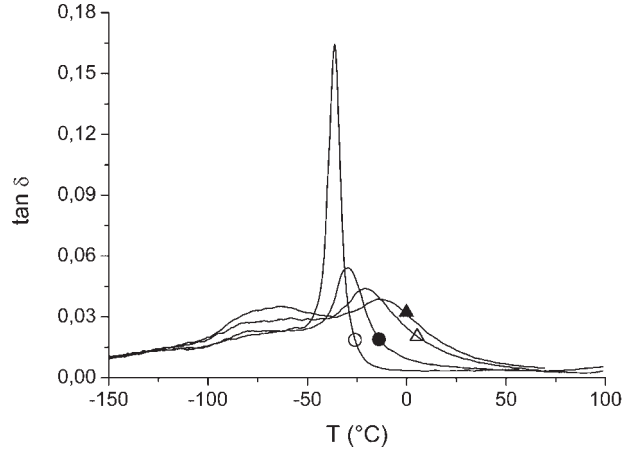

Figure 8. DMTA curves of photocured BEMA1400 (○); of the photocured mixture BEMA1400/HBP (70/30 w/w) (●); of photocured BEMAM-HBP-24 (△) and of the final hybrid Hyb-24-30 (▲), after the dual photocuring and sol-gel reaction.

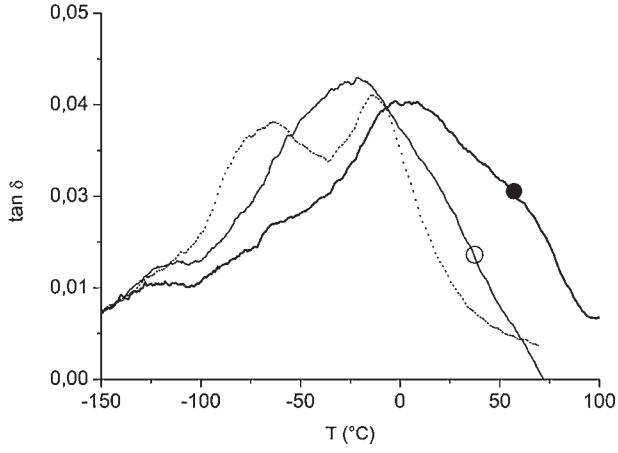

Figure 9. DMTA curves of plasma-treated LDPE (○), of the free hybrid Hyb-24-30 (·····) and of Hyb-24-30 coated on plasma-treated LDPE (●).

Worth noting, however, is the fact that the relaxation spectrum of the hybrid-coated LDPE is by no means the result of simple addition of the loss curves of the two plain constituents. It is quite clear that in the hybrid-coated LDPE, the main relaxation region is shifted to a temperature range higher than that of either plain components. This behavior reflects hindrance to segmental chain mobility and is attributed to adhesion at the substrate/coating interface. Both the visual appearance of the hybrid-coated LDPE films and their mechanical performance during manipulation support the idea that polymer film and coating are coupled via good interfacial adhesion.

An analogous behavior was recently reported for hybrids similar to the present ones, but lacking the hyperbranched component coated on PET films.[14] Unlike the present LDPE, the PET substrate did not show any dynamic-mechanical losses in the temperature range of the hybrid main relaxation, hence attribution of the observed relaxation behavior changes could be unambiguously assigned to the ceramer. In the earlier study, the hybrid glass transition underwent a thickness-sensitive, very clear up-shift upon coating on PET that was straightforwardly ascribed to adhesion of the ceramer to the supporting polymer.[14]

In addition to DMTA, mechanical tensile tests were also performed in order to evaluate adhesion of the hybrid coating onto plasma treated LDPE films. Figure 10 displays stress-strain curves of LDPE and LDPE coated with Hyb-24-70, which should be among the less ductile synthesized hybrids, due to the high amount of TEOS present in its formulation. The two systems show a similar behavior up to a strain of 8.5%. The elastic moduli of LDPE and of the coated material were evaluated measuring the initial slope of the experimental curves. Values of 120 MPa were obtained for both, indicating that the modulus of the coating is close to that of LDPE.

At higher strains ($\varepsilon \geq 8.5\%$), a significant slope variation can be observed for LDPE, due to material's yielding. The coated material, instead, shows a lower deformability than LDPE. No damage of the coating was observed up to $\varepsilon = 20\%$. At a higher strain, a fast decrease of stress takes place, due to coating's fracture, as shown in Figure 11, where stress is plotted versus testing time for both LDPE and LDPE coated with Hyb-24-70: indeed, it can be observed that at $t > 400$ s, the loading curve of the coated material suddenly drops to that of LDPE. When fracture takes place, a total detachment of the coating from the substrate is observed.

The foregoing mechanical experiments lead to the following conclusions: (a) the modulus of the coating is

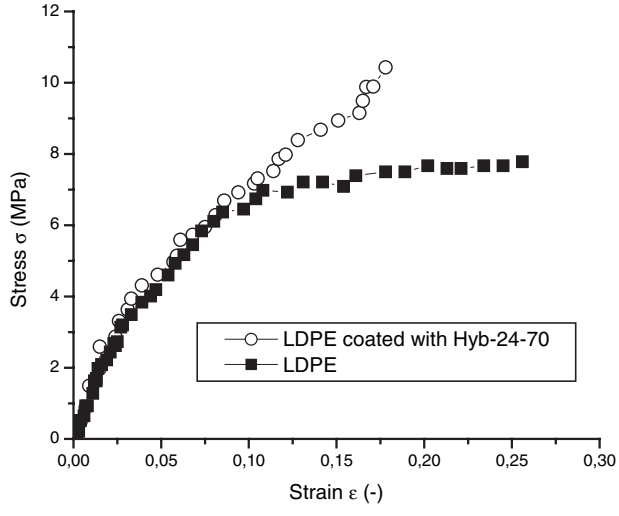

Figure 10. Stress-strain curves of LDPE and LDPE coated with Hyb-24-70 at 4.5×10^{-3} s^{-1}.

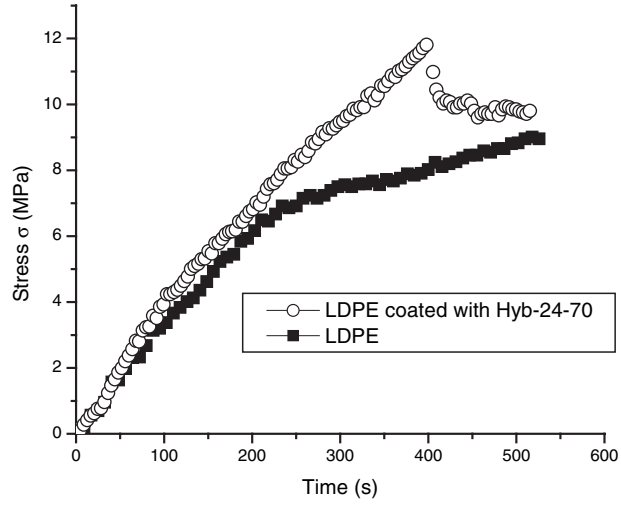

Figure 11. Stress versus time plot of LDPE and LDPE coated with Hyb-24-70 at 4.5×10^{-3} s^{-1}.

similar to that of LDPE; (b) coating strength is higher than that of LDPE and coating fracture takes place catastrophically at a strain well above 20%; (c) the coating adheres to LDPE until it fractures, though no quantification of the adhesive stress is possible from these preliminary experiments.

Conclusion

The influence of addition of a HBP, bearing acrylic groups to a system containing an acrylate PEO oligomer and TEOS in the presence of MEMO as phase linker was analyzed during hybrid formation through UV-curing and condensation. The kinetics of the photopolymerization reaction was found to be affected by the high crosslink functionality of HBP.

The thermal and viscoelastic properties of the hybrid films, investigated by DSC and DMTA, show that during the dual curing process, temperature and width of the organic phase glass transition increase, while the transition intensity decreases. The changes are correlated with the various crosslinking steps. The presence of the multifunctional HBP reactant enhances this effect. Both DMTA and mechanical experiments evidence good adhesion of the hybrid coatings to plasma-treated LDPE. The highest inorganic content coating investigated (70% TEOS in hybrid feed) had a strength higher than that of LDPE and fractured (with consequent detachment from substrate) at a strain well above 20%. This latter feature may have interesting implications in packaging applications.

Acknowledgements: The financial support of *MIUR* (PRIN 2004, Prot. 2004030304) is gratefully acknowledged.

[1] J. Wen, G. L. Wilkes, *Chem. Mat.* **1996**, *8*, 1667.
[2] S. Yano, K. Iwata, K. Kurita, *Mater. Sci. Eng. C* **1998**, *6*, 75.
[3] M. Ochi, R. Takahashi, A. Tenanchi, *Polymer* **2001**, *42*, 5151.
[4] L. Mascia, *Trends Polym. Sci.* **1995**, *3*, 61.
[5] J. Lange, Y. Wyser, *Package Technol. Sci.* **2003**, *16*, 149.
[6] G. Kickelbick, *Prog. Polym. Sci.* **2003**, *28*, 83.
[7] D. Tian, P. Dubois, R. Jerome, *J Polym. Sci., Part A: Polym. Chem.* **1997**, *35*, 2295.
[8] D. Tian, P. Dubois, R. Jerome, *Polymer* **1996**, *37*, 3983.
[9] D. Tian, S. Blancher, P. Dubois, R. Jerome, *Polymer* **1998**, *39*, 855.
[10] K. Zou, M. D. Soucek, *Macromol. Chem. Phys.* **2004**, *205*, 2032.
[11] J. Cho, H. Ju, J. Hong, *J Polym. Sci., Part A: Polym. Chem.* **2005**, *43*, 658.
[12] H. J. Glasel, F. Bauer, H. Ernst, M. Findeisen, E. Hartmann, H. Langguth, R. Mehnert, R. Schubert, *Macromol. Chem. Phys.* **2000**, *201*, 2765.
[13] G. Malucelli, A. Priola, M. Sangermano, E. Amerio, E. Zini, E. Fabbri, *Polymer* **2005**, *46*, 2872.
[14] G. Ceccorulli, E. Zini, M. Scandola, *Macromol. Chem. Phys.* **2006**, *207*, 864.
[15] J. G. Kloosterboer, *Adv. Pol. Sci.* **1988**, *84*, 1.
[16] M. Johansson, A. Hult, *J. Coat. Tech.* **1995**, *67*, 849.
[17] M. Trollsas, C. J. Hawker, J. F. Remenar, J. L. Hedrick, M. Johansson, H. Ihre, A. Hult, *J. Polym. Sci., Polym. Chem. Ed.* **1998**, *36*, 2793.
[18] K. Dusek, M. Duskova-Smrckova, "*Formation, Structure and Properties of the Crosslinked State Related to Precursors Architecture in Dendritic Polymers*" D. A. Tomalia, J. M. Frechet, Eds., Wiley-VCH, Weinheim 2002, p. 111.
[19] W. F. Shi, B. Ranby, *J. Appl. Polym. Sci.* **1996**, *59*, 1937.
[20] M. Johansson, E. Malmstrom, A. Hult, *J. Polym. Sci., Part A: Polym. Chem.* **1993**, *31*, 619.
[21] M. Sangermano, G. Malucelli, R. Bongiovanni, A. Priola, A. Harden, *Polym. Int.* **2005**, *54*, 917.
[22] M. Sangermano, A. Di Gianni, G. Malucelli, C. Roncuzzi, A. Priola, B. Voit, *J. Appl. Polym. Sci.* **2005**, *97*, 293.
[23] N. G. McCrum, B. E. Read, G. Williams, "*Anelastic and Dielectric Effects in Polymeric Solids*", Wiley, New York 1967, Chapter 13.
[24] "*Polymeric Materials Encyclopedia*", M. Pizzoli, M. Scandola, J. C. Salamone, Eds., CRC Press Inc., Boca Raton **1996**, Vol. 7, pp. 5301–5308.
[25] J. Kolarik, J. Janacek, *J Polym. Sci., Part C* **1967**, *16*, 441.
[26] H. W. Starkweather, Jr,. "*Water in Nylon in Water in Polymers*", S. P. Rowland, Ed., American Chemical Society, Washington 1980.

